RESEARCH PAPER

Ease Synthesis of Broccoli -Like Fe_3O_4 Nanostructures for Superior Removal of Eosin Yellow Dye

Hussein M. Mohammad , Shaymaa I. Saeed, Luma M. Ahmed *

Department of Chemistry, College of Science, University of Kerbala,56001, Iraq

ABSTRACT

Due to its crucial function in environmental cleanup, superparamagnetic iron oxide nanoparticles continue to be the topic of intensive research in the present day. The elimination of textile effluent dye is the subject of the current investigation. Inverse spinel (Fe_2O_3. FeO) was produced as magnetic iron oxide (Fe_3O_4) nanoparticles using an unique precipitation approach that relied on the preparation of the particles without any calcination under oxygen gas. The iron sulfate solution was combined with an aqueous mixture of sodium hydroxide and sodium nitrate to create the Fe_3O_4 nanoparticles, both without and with the use of surfactant like cetramide as templates. FT-IR spectra showed that Fe-O octahedral and tetrahedral bindings at 744 cm^{-1} and 598 cm^{-1}, respectively, indicated to form an inverse spinel particle. The X-ray diffraction (XRD) research explained that the mean crystal size of Fe_3O_4 nanoparticle increased from 8.5 nm for Fe_3O_4 nanoparticle to 22.53 nm for prepared Fe_3O_4 in presence of cetramide as a template. SEM found the produced shapes as spherical like brooklei. The thermodynamic analysis demonstrated that prepared Fe_3O_4 in the presence of cetramide underwent endothermic adsorption with chemisorption, while the magnetite prepared without using cetramide is exothermic with physisorption. The magnetite with cetramide a better fit for Freundlich model, and proved it chemisorption. The findings showed that Fe_3O_4 produced with cetramide is a better adsorbent for removing anionic dye and it is utilized to remove water contaminants.

INTRODUCTION

Numerous practical uses for nanotechnological materials have attracted researchers to this topic [1]. One of the most prevalent types of magnetic nanoparticles (NPs) is enticing nanomaterials with a wide range of uses, particularly in the fields of magnetic data storage, magnetic resonance imaging, magneticuids, biotechnology/biomedicine, high performance inductors, catalysis, and environmental cleanup. Nanomaterials are frequently governed by their properties and uses [2-4]. Rapid development is occurring in nanotechnology. The growing usage of nanotechnology products, especially for biomedical applications, has also sparked worries about the emergence of unanticipated adverse health effects following exposure. It is crucial to comprehend the toxicological profiles of engineered nanomaterials to guarantee that

* *Corresponding Author Email: luma.ahmed@uokerbala.edu.iq*

these materials are safe for use and are ethically produced with a focus on benefits and a reduction in risks. However, the creation and manufacture of engineered nanomaterial's are growing more quickly than the production of toxicological data [1]. Magnetic IONPs are frequently employed as drug carriers in the treatment of cancer [6, 7], magnetic resonance imaging (MRI) agents [8, 9], bio-separation [10, 11], gene delivery [12, 13], biosensors [14, 15], protein purification [16, 17], immunoassays [18, 19], and cell labeling [20, 22]. This is based on recent research and published literature. They are commonly employed in the management of hyperthermia [22, 23]. The three forms of iron oxides that are most frequently found in nature are magnetite (Fe$_3$O$_4$), magnetite (Fe$_2$O$_3$), and hematite (Fe$_2$O$_3$). These oxides will be the subject of this examination because they are also essential to scientific advances. Super para-magnetism, a special form of magnetism, is displayed by NPs manufactured of ferromagnetic materials and measuring 10–20 nm or less [24]. An adequate statistical description is particularly challenging when it comes to solid materials because of their variability, including porous adsorbents, which make up the majority of industrial adsorbents. Under the assumption that the surface and bulk phases are in thermodynamic equilibrium, we can generate various adsorption isotherms by employing the equality of the chemical potentials of a specific component in coexisting phases. How these equations can be analytically represented depends on the proposed models for the surface and bulk phases. The surface phase can be classified as monolayer or multilayer, confined, mobile, or partially mobile. The analytical forms of adsorption isotherms are difficult to understand because solid surfaces have structural and energetic heterogeneity, which is a characteristic of a wide range of adsorbents used in practice [25, 26].

The equilibrium between a bulk phase and the surface layer can be attained with reference to neutral or ionic particles. Ion exchange is a process in which an equal number of ionic species are concurrently adsorbed and desorbed. Physical adsorption, also known as physisorption or universal van der Waals interactions can both lead to adsorption. Alternatively, it could resemble a chemical process, such as chemical adsorption or chemisorption. Chemisorption, a contrast to physisorption, only takes place as a monolayer[2].

That will similar to the physical adsorption to the adsorptive condensation process. It often happens at a temperature below or very near the critical temperature of an adsorbed material and is reversible. Therefore, the current study is aimed to synthesize and characterize two prepared types of magnetic iron oxide nanoparticles with and without using of cetramide. Both prepared iron oxide nanoparticles were investigated and compared considering different factors such as FT-IR, XRD, SEM and EDX spectra. The effect of dye concentration was also used to assess the adsorption kinetics and isotherms. Moreover, the acquired experimental findings were used to determine the thermodynamic parameters ($\Delta G°$, $\Delta H°$, and $\Delta S°$).

MATERIALS AND METHODS

Materials

In this experiment, the sodium nitrate NaNO$_3$, sodium hydroxide NaOH, and ferric sulfate FeSO$_4$.7H$_2$O were used all provided by BDH. Surfactants like cetramide were supplied by Qualikems. Eosin yellow dye, which provides information as indicated in Table 1, was donated by the CDH.

Synthesis of Spinel Fe$_3$O$_4$ nano crystals

A 2.0 g of FeSO$_4$•7H$_2$O was put in 400 mL beaker size and then had been dissolved in 150 mL of water. A 50 mg of NaNO$_3$ and 0.56 g of NaOH were transferred to 100 mL beaker size, and then dissolved in 60 mL of water. The two solutions were heated at 75 °C for 10 minutes. The last solution was mixed with a stirring rod rather than a magnetic stir bar. The resulting heated solution was picked up with a tong. The suspension initially turned green before quickly turning black. The black color suspension was continuously heated to 90 °C for ten minutes, and then cooled to 20 °C before being acidified with three millilitres of concentration HCl. This murky fluid was filtered by the Buchner funnel. The Buchner funnel was used to filter this dark solution.

The resulting black precipitate was washed twice with 50 mL of water to get rid of all the salts, and it was then dried in the oven at 100 °C for 60 minutes. As depicted in Fig. 1, the black powder was scraped from the filter paper. The chemical reactions of spinel Fe$_3$O$_4$ formed without and with surfactant were suggested using the following equations.
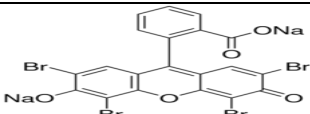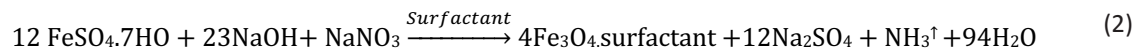
$$12 \, FeSO_4.7HO + 23NaOH + NaNO_3 \rightarrow 4Fe_3O_4 + 12Na_2SO_4 + NH_3^{\uparrow} + 94H_2O \qquad (1)$$

$$12 \, FeSO_4.7HO + 23NaOH + NaNO_3 \xrightarrow{Surfactant} 4Fe_3O_4.surfactant + 12Na_2SO_4 + NH_3^{\uparrow} + 94H_2O \qquad (2)$$

Table 1. The General properties of Eosin yellow dye [3].

Hill Formula	Molar mass g/mole	Dye class	Colour	λ_{max} /nm.	Structure
C$_{20}$H$_6$Br$_4$Na$_2$O$_5$	691.9	Xanthene dye	Pink powder and slightly yellowish cast in aqueous solution	516	

Removal of Eosin yellow dye using synthesized spinel Fe$_3$O$_4$

The 0.01 g of prepared Fe$_3$O$_4$ samples with the 6.5 pH was added to 5 mL of the 10 mg/L the eosin yellow dye solution in the beaker. This solution was shaken with a shaker for 10 to 60 minutes at 50 rpm and 22 °C. Both were taken up by the magnet after the dye had been adsorbed on the Fe$_3$O$_4$ surface. Using a UV-visible spectrophotometer set to measure the absorbance of solution after adsorption at 516 nm, the amount of adsorption C$_e$ was determined by measuring the residual dye concentration after adsorption depended on the calibration curve. Equation 3 was used to calculate the dye removal quantity of absorption (q$_m$)[3, 4] using various types of produced nanoparticles.

$$q_m = \frac{(C_O - C_T) * V}{m} \qquad (3)$$

RESULTS AND DISCUSSION
Synthesis of Iron oxide NPS

The major goal of this work was to create magnetic iron oxide utilizing hydrated iron sulphate without and with the addition of a surfactant like
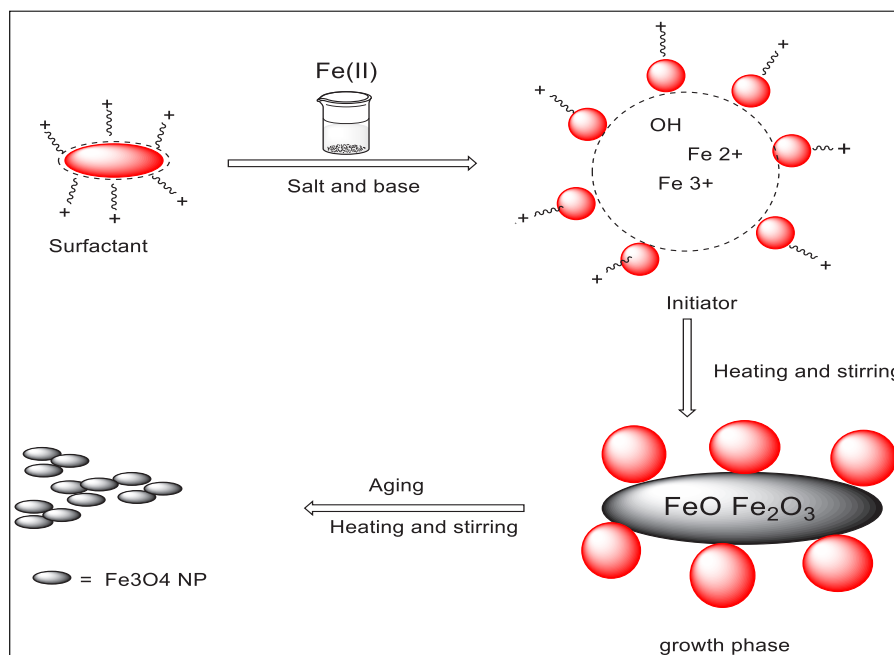

Fig. 1. Schematic diagram for enhanced the magnetic iron oxide NP preparation in presence of surfactants (adapted from the reference) [4].
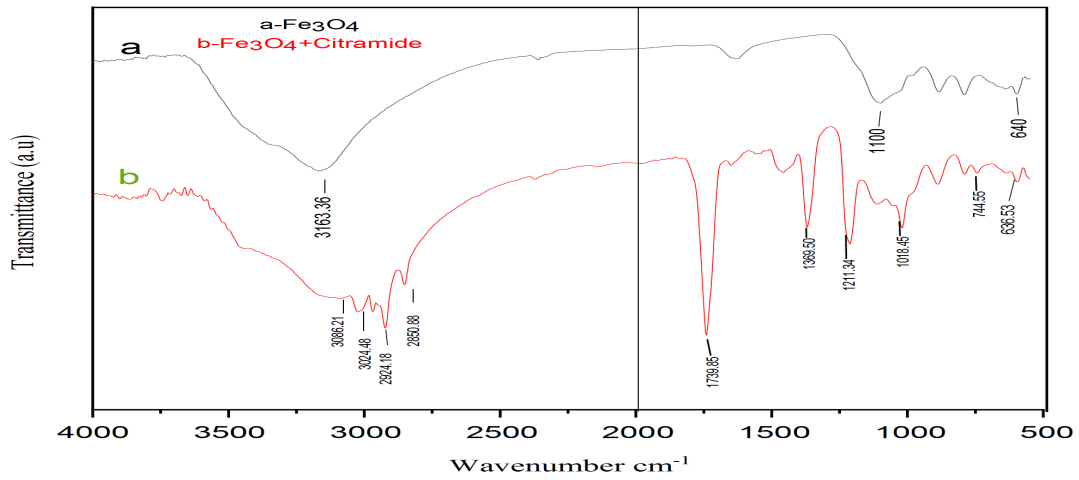
Fig. 2. The FT-IR spectrum of (a) Fe$_3$O$_4$ and (b) Fe$_3$O$_4$ + Cetramide

cetramide. Some Fe(II) was changed to Fe(III) by partially oxidizing it with sodium nitrate while also being in the presence of a base medium made of NaOH. To ensure appropriate growth, the general method of organizing the prepared Fe$_3$O$_4$ NP in the presence of surfactant as template was examined.

Characterization of the prepared Fe$_3$O$_4$ nanoparticles

A. FT-IR Analysis

FTIR spectra appeared for magnets prepared in Fig. 2 without and with using cetramide. The black line (a) for spinal Fe$_3$O$_4$ occur the wide peak at 3163.36 cm^{-1} belonging the O - H group, in addition to the peak at 1100 cm^{-1} explaining the O-Fe-O as an octahedron bending. As for the Fe-O bonding, it is in locations between 640 cm^{-1} and 598 cm^{-1} that present the tetrahedral curvature. The red line (b) for Fe$_3$O$_4$ + cetramide shows the broad peak at 3082 cm^{-1} beyond the O–H stretching of the iron oxide. This decrease in wave number refers to a decrease the energy and an increase the stability after addition cetramide as positive surfactant. Another peak at 3028 cm^{-1} assigned to the N–H
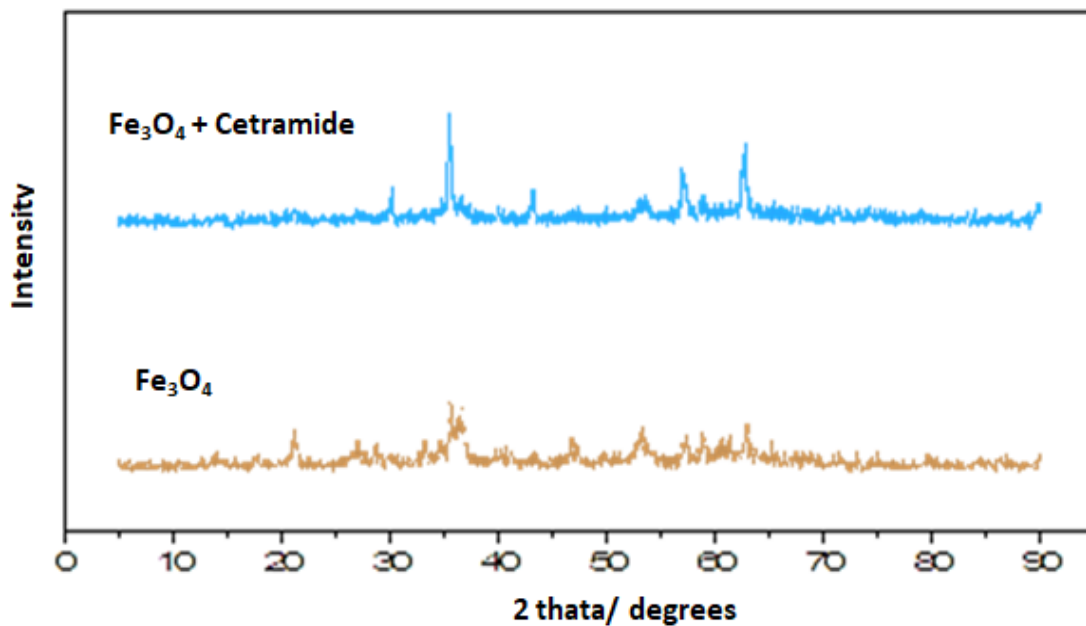

Fig. 3. XRD spectra of prepared Fe$_3$O$_4$ without and with using cetramide as surfactants (Fe$_3$O$_4$+Cetramide).

bending in addition to the peaks between 2924 cm⁻¹ and 2850 cm⁻¹ represent stretching C-H. The peak at 1211 cm⁻¹ explains the O–H bending. The more intense bands between 744 cm⁻¹ and 598 cm⁻¹ represent to Fe-O octahedral and tetrahedral bending [5].

Structure Property

X-ray diffraction (XRD) measurements in Fig. 3 (black and blue lines) were used to obtain the crystal structure of the prepared magnetic iron oxide nanoparticle without and with of cetramide surfactant respectively. The appearance of diffraction peaks at 2θ values of 18.96°(111), 30.4° (220), 35.64° (311), 43.4° (400), 53.16° (422), 57.32° (511), 63.12 ° (440), and 73.12° (553) are consistent with the standard XRD data of the structure of spinel Fe₃O₄. It was also observed

that some values disappeared and their relative intensity changed with use of surfactants, where the peak at 2θ values of 18.96 ° (111) disappeared when using cetrimide. The increase in the relative strength of the 35.64 ° peaks. (311), 43.4 ° (400), 53.16 ° (422), 57.32 ° (511), 63.12° (440), and 73.12 ° (553) the prepared nanoparticles in the case of using ceramide. The magnetite nanoparticles for all shapes in Fig. 3 (a&b) are well crystalline and the position and the relative intensity of the diffraction peaks match well with the standard phase magnetite NPs diffraction pattern of the International Center of Diffraction Data card (JCPDS No. 19-0629)[6].

The mean crystal sizes (D) of the synthesized magnetite nanoparticles without and with the presence of surfactants were calculated using
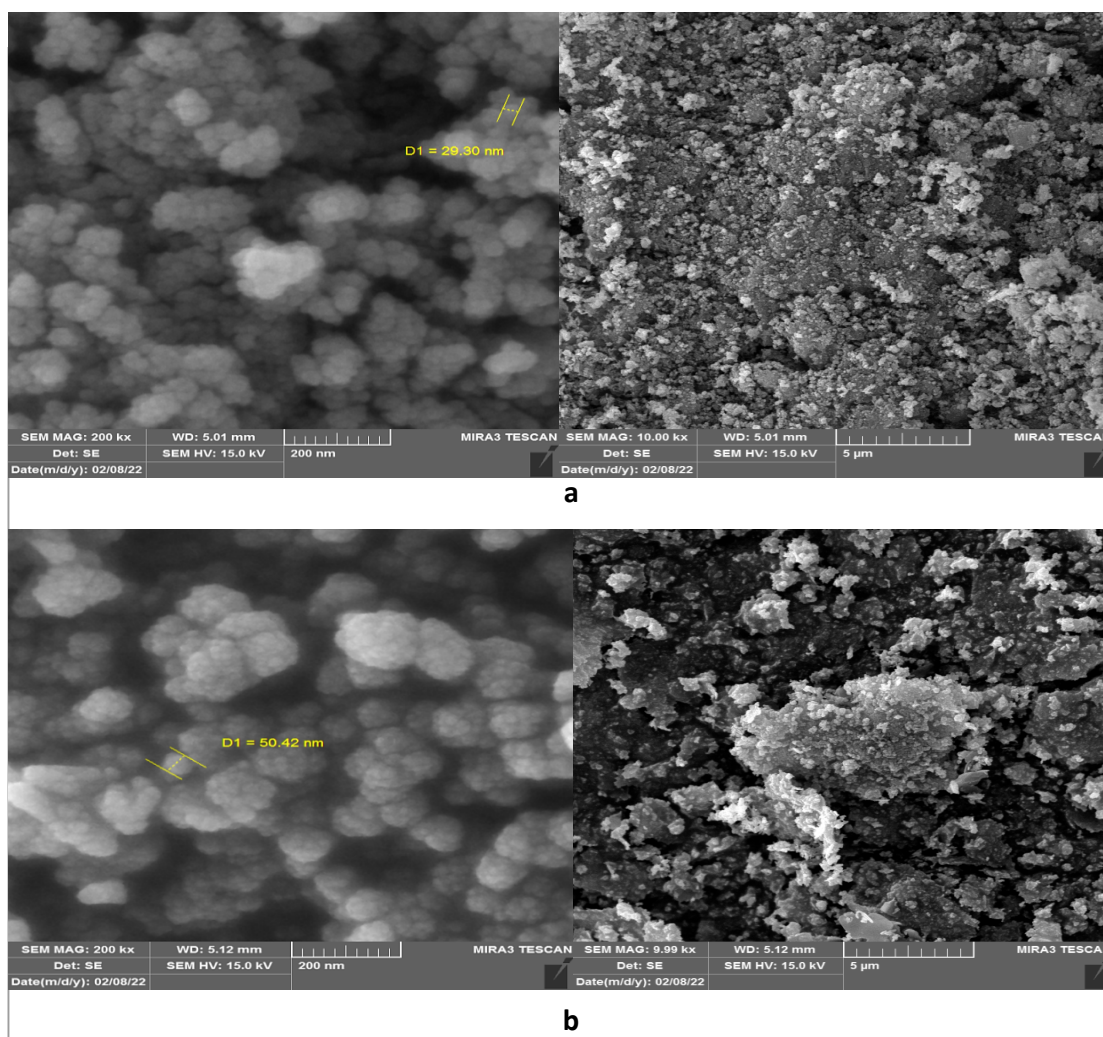

Fig. 4. The scanning electron microscope (SEM) analysis of (a) Fe₃O₄ and (b) Fe₃O₄ + cetramide.

Table 2. Compares Langmuir models between Fe_3O_4 without and with using cetramide as a surfactant.

Modulse	Langmuir for Fe_3O_4	Langmuir for Fe_3O_4 + cetramide
K_L (L/mg)	1.60×10^2	-120.403
q_{max} (mg/g)	244.498	0.431
(R_L) R^2	0.495	0.640

Debye-Scherer formula [7].

$$D = \frac{K\lambda}{\beta \cos\theta} \quad (4)$$

Where β is the full width at half-maximum value of XRD diffraction lines, λ is the wavelength of X-ray radiation source 0.15405 nm. β = the half diffraction angle –Bragg angle and k refers to the Scherer constant with a value from 0.85 to 0.94. The mean crystal size of iron oxide NP without cetramide was 8.5 nm regarded as a quantum dote nanoparticle because its size value is less than 10 nm, this value is the same as another nanoparticles studies reported in references [8]. However, after adding the cetramid surfactant during iron oxide NP preparation, the mean crystal size increases from 8.5 nm to 22.53 nm due to the behavior of surfactants as a template.

SEM analysis

One of the most important techniques for studying various surfaces and the changes that occur on them is the scanning electron microscope (SEM) in Fig. 4.

According to Fig. 4 (a & b) for SEM analysis, the particle size of iron oxide NP without and with

the use of cetramide surfactant increased with the following sequences: 20.30 nm and 50.42 nm respectively. This behavior indicates that all prepared NP without and with using of cetramide surfactant are polycrystals; these findings are consistent with other findings reported in [9, 10].

Sorption isotherm model

Adsorption isotherms are thought to be one of the most important requirements for determining the relationship between adsorbent and adsorbate. They are also of high quality, highlighting the significance of achieving and the most effective dyeing style removal [11]. Furthermore, they are critical in explaining particle distribution between the two phases in the equilibrium state, and there are several models available. It has been used in the literature by Langmuir, Freundlich, and others [11]. This study employed the Langmuir and Freundlich models, which were chosen as follows: The Langmuir isotherm equation[12].

$$q_e = \frac{q_m \quad KaCe}{1 + KaCe} \quad (5)$$

Where q_e is the amount absorbable per unit mass of sorbent material at equilibrium (mg/g), q_m is the maximum sorption capability
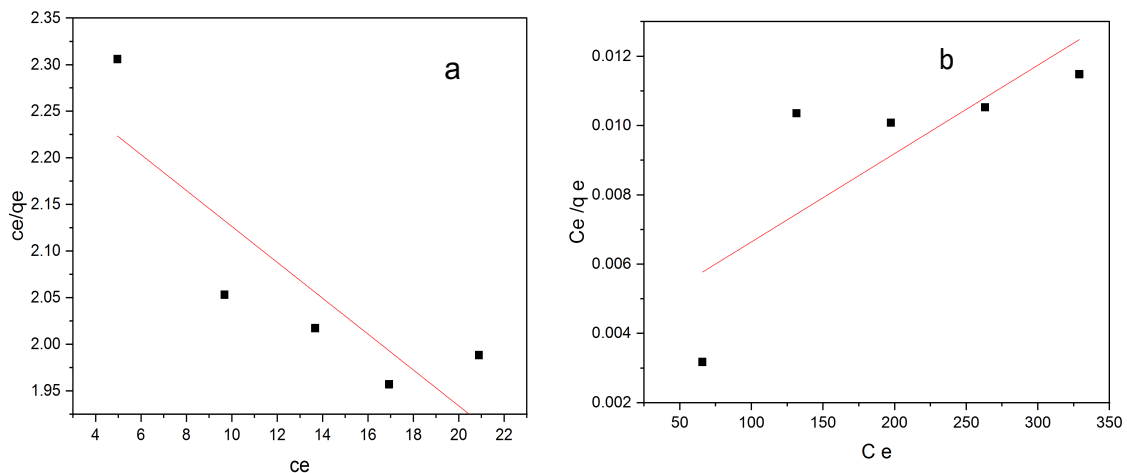

Fig. 5. Langmuir equation plots for (a) Fe_3O_4 NPS and (b) Fe_3O_4 NPS with the cetramide.

Table 3. Comparism Freundlich models between Fe_3O_4 without and with using cetramide as surfactant.

Modulse	Freundlich equation for Fe_3O_4	Freundlich equation for Fe_3O_4 + cetramide
$K_f = (mg\ g^{-1})(L\ mg^{-1})^{1/n}$	152.328	0.338
n (g/L)	1.283	0.864
R^2	0.526	0.999

(mg/g), Magnetite nanoparticle concentration at equilibrium (Ce) is measured in mg/L., and K_a is the sorption constant. In equation (6), the plot of Ce/qe versus Ce is linear.

$$\frac{Ce}{qe} = \frac{1}{qeKa} + \frac{Ce}{qm} \qquad (6)$$

The essential characteristics of the Langmuir model can be defined by a dimensional constant known as the equilibrium parameter, R_L [14] ,which is definite by:

$$R_L = \frac{1}{1 + b\ C_o} \qquad (7)$$

Where b represents the Irving Langmuir constant

and Co represents the initial concentration of dye, the value of R_L (R^2) indicates whether the line is unlucky ($R_L > 1$), linear ($R_L = 1$) and permanent ($R_L = 0$).

As results, the dye sorption onto Fe_3O_4 with and without cetramide surfaces was occurred in table 2.

The Freundlich isotherm equation[13] was applied as equation 8.

$$Log\ qe\ = \frac{1}{n} logCe + \log Kf \qquad (8)$$

Where q_e is the amount of adsorbate per unit mass of adsorbent at equilibrium (mg/g) and C_e is the solution's equilibrium of dye (mg/L). K_f and
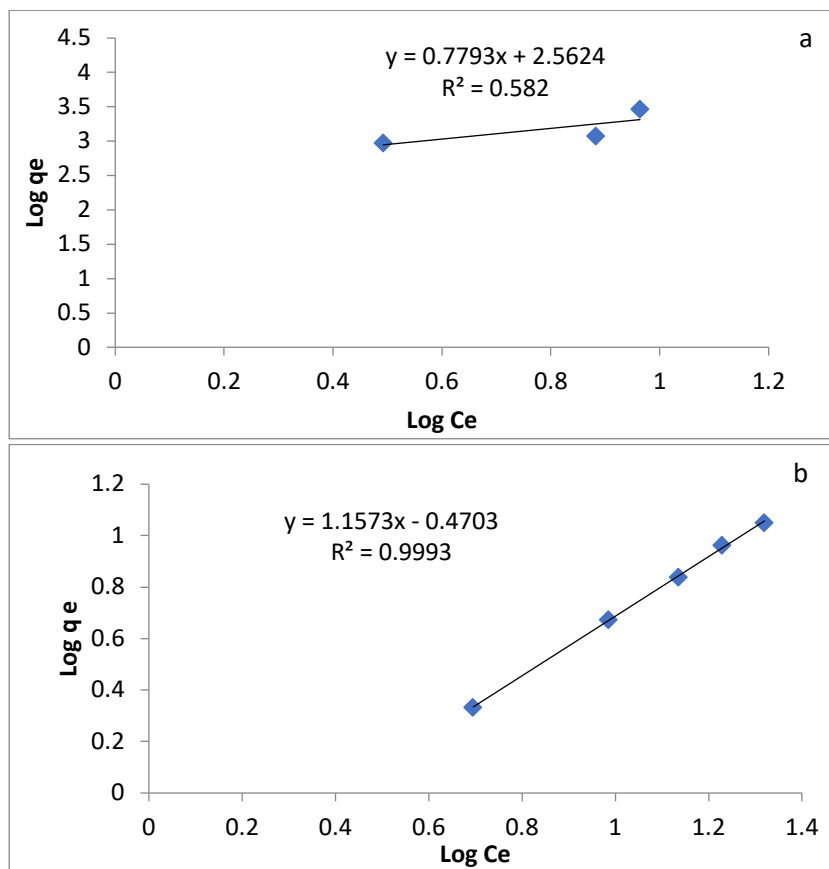

Fig. 6. Freundlich equation plots for (a) Fe_3O_4 NPS and (b) Fe_3O_4 NPS with the cetramide.

Table 4. The Kinetic and Thermodynamic Parameters for Adsorption of Eosin Yellow Dye on Fe₃O₄ Surface that prepared in presence and absence cetramide with temperature range (278-303) K.

Modulse	T/K	$\Delta H°$ kJ mol^{-1}	$\Delta S°$ kJ mol^{-1}	$\Delta G°$ kJ mol^{-1}	E_a kJ mol^{-1}
Fe₃O₄ with cetramide	278			-3.273	39.040
	288			-5.463	39.124
	298	36.729	0.144	-6.134	39.207
	303			-7.122	39.248
Fe₃O₄ without cetramide	288			27.119	-147.433
	293			27.673	-147.391
	298	-149.827	-0.5073	28.229	-147.349
	303			28.787	-147.308

n are the Freundlich constants, with n providing a sign of favorability and K_f = (mg g^{-1})(L mg^{-1})$^{1/n}$. The values of K_f and n are obtained from the log q_e versus log C_e plot in Fig. 5, and they are capable of calculating the intercept and slope of the several times. The n value is near 1 for adsorption of dye

on prepared Fe₃O₄ using cetramide that indicates to chemisorption and Freundlich model is more obeyed than Langmuir equation. As shown in Fig. 5 and 6 and listed in Tables 2 and 3. The adsorption process of dye using prepared Fe₃O₄ without and with using cetramide as surfactant is found to

y = -4.4178x + 17.401
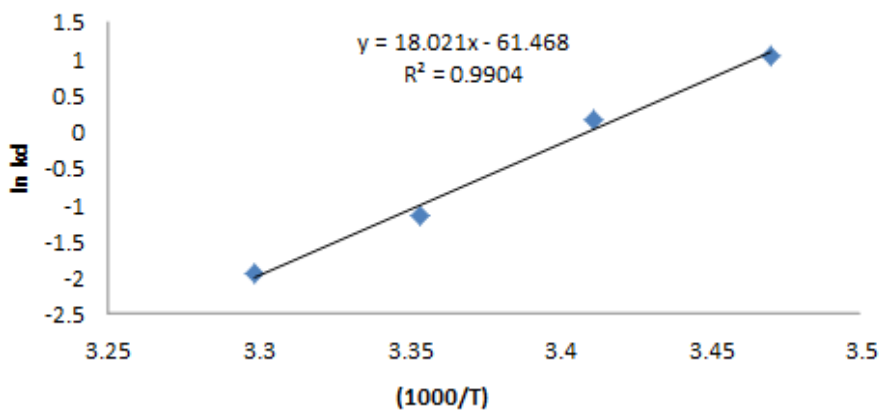R² = 0.938

a

y = 18.021x - 61.468
R² = 0.9904
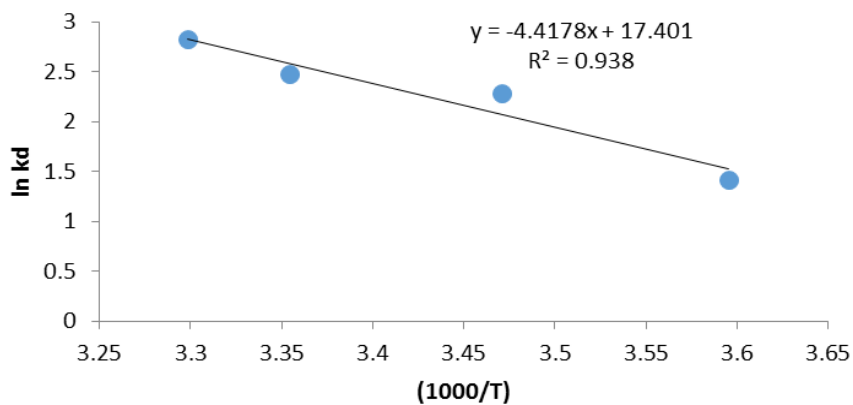
Fig. 7. Compares between shape relation between ln k_d adsorption of eosin yellow dye on Fe₃O₄ surface that prepared (a) in absence cetramide and (b) in presence cetramide as a surfactant at 1h.
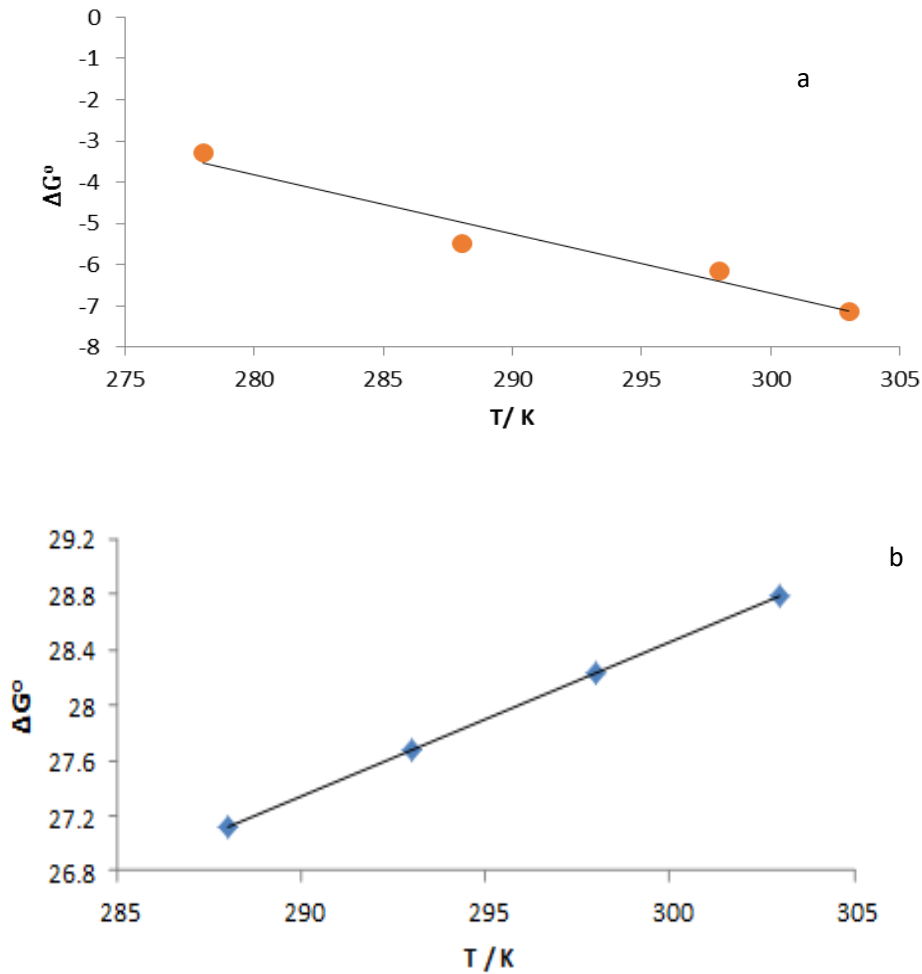
Fig. 8. (a) Relation of Gibb's free energy change (ΔG°) versus temperature for an endothermic process of adsorption of eosin yellow dye on Fe$_3$O$_4$ surface that prepared in presence cetramide as a surfactant and (b) exothermic process in absence cetramide, (a) and (b) in temperature ranged (278.15-303.15) K at 1h.

be physical adsorption and chemical adsorption, respectively.

The Kinetic and thermodynamic studies of removal of eosin yellow dye using Fe$_3$O$_4$ NPS without and with cetramide

The thermodynamic parameters are critical in determining the type of adsorption process that occurred on any solid surface. To begin, the sorption distribution coefficient (k_d) [14, 15]was calculated using equation 9, where $C_{ads.}$ is the amount of adsorbate (dye) on the solid surface (prepared Fe$_3$O$_4$ without and with using cetramide) at equilibrium (mg/L), and Ce is a residual dye (mg/L) in an equilibrium solution. The Gibbs energy (ΔG⁰) was calculated using equation 10 (Gibbs

equation), where R is the universal gas constant (J/mol K) and T is the absolute temperature in (K).

$$k_d = \frac{C_{ads.}}{C_e} \qquad (9)$$

$$\Delta G^o = -RT ln k_d \qquad (10)$$

The difference in enthalpy ΔH° and entropy ΔS° were measured using the Van't Hoff equation [16, 17]. (equation 11).

$$ln k_d = \frac{-\Delta H^o}{RT} + \left(\frac{\Delta S^o}{R}\right) \qquad (11)$$

On the other hand, the activation energy (E$_a$) was determined using equation 12 [4, 17].

$$E_a = \Delta H^o + RT \qquad (12)$$

There are comperes between magnetite with and without surfactant, for Fe$_3$O$_4$ prepared by cetramide as the findings in Figs. 7 and 8. The results in Table 4 determined that the eosin yellow dye's adsorption process on the surface of the Fe$_3$O$_4$ using cetramide is endothermic in nature and has a positive magnitude of ΔH^o value equal to (36.729 kJ mol^{-1}). This result, which is greater than (4.2) kJ mol^{-1} [16], indicates that the adsorption mechanism is chemisorption. Furthermore, the ΔS^o magnitudes are little and positive (0.14467 kJ mol^{-1}), which suggests that there is an increase in randomness at the solid/solution interface. The fact that the activation energies in Table 4 are positive and rise as temperature rises, from (39.040 to 39.248) kJ mol^{-1}, that indicates to the process is chemisorption, due to the activation energies having a range between 8.4 kJ mol^{-1} and 83.7 kJ mol^{-1} [16]. That the process of adsorption occurs as a result of a change in the internal structure [16, 18]. In Fig. 8, the ΔG^o demonstrated that the adsorption reaction of dye on prepared Fe$_3$O$_4$ using cetramide is also endothermic; this result is in agreement with that report in [46].

According to using the prepared Fe$_3$O$_4$ without cetramide, the findings in Fig. 7 and Table 4, it is determined that the eosin yellow dye's adsorption process on the surface of the prepared Fe$_3$O$_4$ without cetramide has a negative magnitude of ΔH^o (exothermic in nature) and is equal to (-149.827 kJ mol^{-1}). This value is found to be less than (4.2) kJ mol^{-1} that indicates that the adsorption process is physisorption. The ΔG^o value is also exothermic; as shown in Fig. 8, this result is in agreement with that report in [46]. Additionally, the ΔS^o magnitudes are tiny and negative (-0.5073 kJ mol^{-1}), implying that there is a decrease in randomness at the solid/solution interface and that the mechanism of adsorption occurs as a result of a change in the internal structure, hence, sorption process may have occurred. In table, the activation energies are negative values that decrease with a rise in temperature to give a range from (-147.433 to -147.308) kJ mol^{-1}, proving that the process is physisorption because the activation energies value is less (8.4 and 83.7) kJ mol^{-1} and may be multistep can be happened during adsorption.

CONCLUSION

Two distinct magnetite Fe$_3$O$_4$ nanoparticles (NP) were created with and without cetramide. Fe$_3$O$_4$ was shown to exhibit greater adsorption when created it in presence cetramide as a template to improve the growth. On the basis of the locations of the octahedron and tetrahedron peaks, FT-IR analysis determined that the magnetic iron oxide nanoparticle is inverse spinel type. XRD indicated the prepared Fe$_3$O$_4$ NP without cetramide is being as a quantum dot nanoparticle. According to the SEM examination, both samples are nanoparticulate and produced shapes resembling a spherical like brooklei. Because of the prepared Fe$_3$O$_4$ NPs with and without using cetramaide have magnetic properties, so, they used to remove the eosin yellow dye from aqueous solutions. The dye adsorption takes one of two forms: chemisorption; in the case of magnetite with cetramide, while physisorption and sorption for magnetite NP without cetramide. The dye adsorption data were well-fit by the Freundlich models and magnetite prepared in presence of cetramide is better fitted compared the magnetite alone. The strength of the dye's adhesion to the nanoadsorbents was influenced by surfactants. According to the research, iron oxide made with cetramide is a potent adsorbent for absorbing anionic dye and can be used to filter out pollutants from water. The reaction of removal is endothermic using prepared Fe$_3$O$_4$ in presence of cetramide while is exothermic using Fe$_3$O$_4$ alone.

CONFLICT OF INTEREST

The authors declare that there is no conflict of interests regarding the publication of this manuscript.

REFERENCES

1. Bahru TB, Ajebe EG. A Review on Nanotechnology: Analytical Techniques Use and Applications. International Research Journal of Pure and Applied Chemistry. 2019:1-10.
2. Ling W, Wang M, Xiong C, Xie D, Chen Q, Chu X, et al. Synthesis, surface modification, and applications of magnetic iron oxide nanoparticles. J Mater Res. 2019;34(11):1828-1844.
3. Bohara RA, Thorat ND, Pawar SH. Immobilization of cellulase on functionalized cobalt ferrite nanoparticles. Korean J Chem Eng. 2015;33(1):216-222.
4. Jagminas A, Mažeika K, Kondrotas R, Kurtinaitienė M, Jagminienė A, Mikalauskaitė A. Functionalization of Cobalt Ferrite Nanoparticles by a Vitamin C-Assisted Covering with Gold. Nanomaterials and Nanotechnology. 2014;4:11.
5. Valdiglesias V, Fernández-Bertólez N, Kiliç G, Costa C, Costa

S, Fraga S, et al. Are iron oxide nanoparticles safe? Current knowledge and future perspectives. Journal of Trace Elements in Medicine and Biology. 2016;38:53-63.

6. Estelrich J, Escribano E, Queralt J, Busquets M. Iron Oxide Nanoparticles for Magnetically-Guided and Magnetically-Responsive Drug Delivery. Int J Mol Sci. 2015;16(12):8070-8101.

7. Wahajuddin, Arora. Superparamagnetic iron oxide nanoparticles: magnetic nanoplatforms as drug carriers. International Journal of Nanomedicine. 2012;3445.

8. Lee N, Yoo D, Ling D, Cho MH, Hyeon T, Cheon J. Iron Oxide Based Nanoparticles for Multimodal Imaging and Magnetoresponsive Therapy. Chem Rev. 2015;115(19):10637-10689.

9. Kim BH, Lee N, Kim H, An K, Park YI, Choi Y, et al. Large-Scale Synthesis of Uniform and Extremely Small-Sized Iron Oxide Nanoparticles for High-Resolution T1 Magnetic Resonance Imaging Contrast Agents. Journal of the American Chemical Society. 2011;133(32):12624-12631.

10. Fatima H, Kim K-S. Magnetic nanoparticles for bioseparation. Korean J Chem Eng. 2017;34(3):589-599.

11. Zhang G, Qie F, Hou J, Luo S, Luo L, Sun X, et al. One-pot solvothermal method to prepare functionalized Fe₃O₄ nanoparticles for bioseparation. J Mater Res. 2012;27(7):1006-1013.

12. Jiang S, Eltoukhy AA, Love KT, Langer R, Anderson DG. Lipidoid-Coated Iron Oxide Nanoparticles for Efficient DNA and siRNA delivery. Nano Lett. 2013;13(3):1059-1064.

13. Mykhaylyk O, Sobisch T, Almstätter I, Sanchez-Antequera Y, Brandt S, Anton M, et al. Silica-Iron Oxide Magnetic Nanoparticles Modified for Gene Delivery: A Search for Optimum and Quantitative Criteria. Pharm Res. 2012;29(5):1344-1365.

14. Martín M, Salazar P, Villalonga R, Campuzano S, Pingarrón JM, González-Mora JL. Preparation of core–shell Fe₃O₄@poly(dopamine) magnetic nanoparticles for biosensor construction. J Mater Chem B. 2014;2(6):739-746.

15. Baghayeri M, Nazarzadeh Zare E, Mansour Lakouraj M. A simple hydrogen peroxide biosensor based on a novel electro-magnetic poly(p-phenylenediamine)@Fe₃O₄ nanocomposite. Biosensors and Bioelectronics. 2014;55:259-265.

16. Cao M, Li Z, Wang J, Ge W, Yue T, Li R, et al. Food related applications of magnetic iron oxide nanoparticles: Enzyme immobilization, protein purification, and food analysis. Trends in Food Science & Technology. 2012;27(1):47-56.

17. Okoli C, Fornara A, Qin J, Toprak MS, Dalhammar G, Muhammed M, et al. Characterization of Superparamagnetic Iron Oxide Nanoparticles and Its Application in Protein Purification. Journal of Nanoscience and Nanotechnology. 2011;11(11):10201-10206.

18. Peterson RD, Chen W, Cunningham BT, Andrade JE. Enhanced sandwich immunoassay using antibody-functionalized magnetic iron-oxide nanoparticles for extraction and detection of soluble transferrin receptor on a photonic crystal biosensor. Biosensors and Bioelectronics. 2015;74:815-822.

19. Yang M, Guan Y, Yang Y, Xia T, Xiong W, Guo C. A sensitive and rapid immunoassay for mycoplasma pneumonia based on Fe3O4 nanoparticles. Mater Lett. 2014;137:113-116.

20. Li L, Jiang W, Luo K, Song H, Lan F, Wu Y, et al. Superparamagnetic Iron Oxide Nanoparticles as MRI

21. contrast agents for Non-invasive Stem Cell Labeling and Tracking. Theranostics. 2013;3(8):595-615.

21. Soenen SJH, Himmelreich U, Nuytten N, De Cuyper M. Cytotoxic effects of iron oxide nanoparticles and implications for safety in cell labelling. Biomaterials. 2011;32(1):195-205.

22. Bae KH, Park M, Do MJ, Lee N, Ryu JH, Kim GW, et al. Chitosan Oligosaccharide-Stabilized Ferrimagnetic Iron Oxide Nanocubes for Magnetically Modulated Cancer Hyperthermia. ACS Nano. 2012;6(6):5266-5273.

23. Grüttner C, Müller K, Teller J, Westphal F. Synthesis and functionalisation of magnetic nanoparticles for hyperthermia applications. Int J Hyperthermia. 2013;29(8):777-789.

24. Teja AS, Koh P-Y. Synthesis, properties, and applications of magnetic iron oxide nanoparticles. Prog Cryst Growth Charact Mater. 2009;55(1-2):22-45.

25. Dabrowski A, Jaroniec M. Theoretical foundations of physical adsorption from binary non-electrolytic liquid mixtures on solid surfaces: present and future. Advances in Colloid and Interface Science. 1987;27(3-4):211-283.

26. Physical adsorption on heterogeneous solids (Studies in physical and theoretical chemistry #59), M. Jaroniec and R. Madey, Elsevier, Amsterdam (1988) 353 pages Dfl. 250.00 ($131.50). Solid State Ionics. 1990;37(4):327.

27. Adamson AW. Physical adsorption of vapors — three personae. Colloids Surf Physicochem Eng Aspects. 1996;118(3):193-201.

28. Ahmed LM. Photo-Decolourization Kinetics of Acid Red 87 Dye in ZnO Suspension Under Different Types of UV-A Light. Asian J Chem. 2018;30(9):2134-2140.

29. Ding Y, Yang Y, Shao H. High capacity ZnFe₂O4 anode material for lithium ion batteries. Electrochimica Acta. 2011;56(25):9433-9438.

30. Hussain ZA, Fakhri FH, Alesary HF, Ahmed LM. ZnO Based Material as Photocatalyst for Treating the Textile Anthraquinone Derivative Dye (Dispersive Blue 26 Dye): Removal and Photocatalytic Treatment. Journal of Physics: Conference Series. 2020;1664(1):012064.

31. Jawad TM, R. Al-Lami M, Hasan A, Al-Hilifi J, Mohammad R, Ahmed L. Synergistic Effect of dark and photoreactions on the removal and photo-decolorization of azo carmosine dye (E122) as food dye using Rutile- TiO₂ suspension. Egyptian Journal of Chemistry. 2021;0(0):0-0.

32. Alattar R, Saleh H, Al-Hilifi J, Ahmed L. Influence the addition of Fe^{2+} and H_2O_2 on removal and decolorization of textile dye (dispersive yellow 42 dye). Egyptian Journal of Chemistry. 2020;0(0):0-0.

33. Luo X, Liu S, Zhou J, Zhang L. In situ synthesis of Fe₃O₄/cellulose microspheres with magnetic-induced protein delivery. J Mater Chem. 2009;19(21):3538.

34. Porkodi K, Vasanth Kumar K. Equilibrium, kinetics and mechanism modeling and simulation of basic and acid dyes sorption onto jute fiber carbon: Eosin yellow, malachite green and crystal violet single component systems. J Hazard Mater. 2007;143(1-2):311-327.

35. Ramesh AV, Rama Devi D, Mohan Botsa S, Basavaiah K. Facile green synthesis of Fe₃O₄ nanoparticles using aqueous leaf extract of Zanthoxylum armatum DC. for efficient adsorption of methylene blue. Journal of Asian Ceramic Societies. 2018;6(2):145-155.

36. Halbus AF, Hussein FH. Photocatalytic Decolorization of Cobalamin in Aqueous Suspensions of TiO₂ and ZnO Under

Solar Irradiation. Asian J Chem. 2014;26(4):1207-1211.

37. Obaid A, Ahmed L. One-Step Hydrothermal Synthesis of α-MoO$_3$ Nano-belts with Ultrasonic Assist for incorporating TiO$_2$ as a NanoComposite. Egyptian Journal of Chemistry. 2021;0(0):0-0.

38. Hayawi MK, Kareem MM, Ahmed LM. Synthesis of spinel Mn$_3$O$_4$ and spinel Mn$_3$O$_4$/ZrO$_2$ nanocomposites and using them in photo-catalytic decolorization of Fe(ii)-(4,5-diazafluoren-9-one 11) complex. Periódico Tchê Química. 2020;17(34):689-699.

39. Ahmad MA, Ahmad N, Bello OS. Adsorptive Removal of Malachite Green Dye Using Durian Seed-Based Activated Carbon. Water, Air, & Soil Pollution. 2014;225(8).

40. Langmuir I. The adsorption of gases on plane surfaces of glass, mica and platinum. Journal of the American Chemical Society. 1918;40(9):1361-1403.

41. Elshafey E. Sorption of Cd(II) and Se(IV) from aqueous solution using modified rice husk. J Hazard Mater. 2007;147(1-2):546-555.

42. Sadeghi M, Irandoust M, Khorshidi F, Feyzi M, Jafari F, Shojaeimehr T, et al. Removal of Arsenic (III) from natural contaminated water using magnetic nanocomposite: kinetics and isotherm studies. Journal of the Iranian Chemical Society. 2016;13(7):1175-1188.

43. Saha P, Chowdhury S. Insight Into Adsorption Thermodynamics. Thermodynamics: InTech; 2011.

44. Ghazanfari S, Imenshahidi M, Etemad L, Moshiri M, Hosseinzadeh H. Effect of Cyanocobalamin (vitamin B12) in the Induction and Expression of Morphine Tolerance and Dependence in Mice. Drug Res. 2013;64(03):113-117.

45. Zarrouk A, Hammouti B, Zarrok H, Al-Deyab SS, Messali M. Temperature Effect, Activation Energies and Thermodynamic Adsorption Studies of L-Cysteine Methyl Ester Hydrochloride As Copper Corrosion Inhibitor In Nitric Acid 2M. International Journal of Electrochemical Science. 2011;6(12):6261-6274.